

CrystEngComm

Accepted Manuscript



This is an *Accepted Manuscript*, which has been through the Royal Society of Chemistry peer review process and has been accepted for publication.

Accepted Manuscripts are published online shortly after acceptance, before technical editing, formatting and proof reading. Using this free service, authors can make their results available to the community, in citable form, before we publish the edited article. We will replace this *Accepted Manuscript* with the edited and formatted *Advance Article* as soon as it is available.

You can find more information about *Accepted Manuscripts* in the [Information for Authors](#).

Please note that technical editing may introduce minor changes to the text and/or graphics, which may alter content. The journal's standard [Terms & Conditions](#) and the [Ethical guidelines](#) still apply. In no event shall the Royal Society of Chemistry be held responsible for any errors or omissions in this *Accepted Manuscript* or any consequences arising from the use of any information it contains.



Journal Name

ARTICLE

Facile microwave-assisted synthesis and controllable architecture of three-dimensional nickel titanate†

Thuy-Duong Nguyen-Phan,^a Chinh Nguyen Huy,^a Chang-Koo Kim^b and Eun Woo Shin^{*a}

Received 00th January 20xx,
Accepted 00th January 20xx

DOI: 10.1039/x0xx00000x

www.rsc.org/

The rapid, facile, one-pot microwave-assisted polyol synthesis of novel hierarchical nickel titanate (NTN) is first reported in the present study. This method successfully fabricated rhombohedral NiTiO₃ in the shape of a cylindrical storage tank with two elliptical end caps that were constructed from ellipsoid-like nanoparticles. By contrast, irregular NTN aggregates composed of loose granular particles were formed through solvothermal treatment. Varying the dielectric of the solvent with water, n-butanol, acrylic acid, N,N-dimethylformamide, and an EG:butanol mixture significantly affected the crystallographic structure and morphology of the final products due to differences in the loss tangent of each medium under microwave irradiation. Using a nickel source with acetate and halide counterions, which are more readily substituted and have better coordination ability with metal cations than nitrate, resulted in the formation of 3D hexagonal prismatic NiTiO₃ and undesirable 1D rod-like TiO₂ aggregates, respectively. Notably, this study provides a valuable means of developing a rapid, effective method to synthesize NiTiO₃ with uniform morphology, high purity and potential photocatalysis application.

Introduction

ABO₃ ilmenite-type oxides have attracted considerable and still growing attention for a wide range of potential applications due to their excellent dielectric, piezoelectric, pyroelectric, magnetorestrictive, photoelectric, and electro-optical properties.¹ ABO₃-type ilmenite has an ordered corundum structure, where each AO₆ octahedron layer is sandwiched between two BO₆ octahedron layers.¹ In this configuration, the O²⁻ anions have a distorted tetrahedral coordination to four metal cations. Among abundant ternary metal oxides with the ilmenite crystal structure generally formulated as MTiO₃ (M = Fe, Ni, Cu, Sr, Ba, Co, Mn, Pb, Zn), nickel titanate (NiTiO₃), with rhombohedral $R\bar{3}$ symmetry, has a structure in which the Ni and Ti atoms prefer octahedral coordination with alternating cation layers occupied exclusively by Ni²⁺ or Ti⁴⁺.^{2,3} NTN nanomaterials have been prepared by several methods including a modified Pechini process, sol-gel, coprecipitation, flux growth, hydrothermal treatment, combustion, sol-precipitation, electrospinning, solid-state ceramic, pyrolysis of polymeric precursors, and wet chemical synthesis (using

citrate, maleate, propionic acid or stearic acid).^{3,4-12}

Similar to other perovskite-like compounds, NTN is extensively employed in ceramics and cool pigments as well as in solid lubricants (as a tribological coating to reduce friction and wear in high temperature applications).⁴⁻⁶ NTN materials have also been utilized as semiconductor rectifiers, electrodes for solid oxide fuel cells, gas sensors, and metal-air barriers.¹³⁻¹⁶ In particular, due to a narrow band gap (2.1 ~ 2.2 eV) and *n*-type nature, NTN materials have been widely used as visible light-driven photocatalysts.^{2,3,12,17-19}

However, aside from complicated routes, the syntheses of NTN materials have a variety of inherent problems, such as generating material with large particle size, uncontrolled morphology, and low purity, poor reproducibility and uniformity due to high sintering temperature, and heterogeneous solid phase reactions.⁴⁻¹² A few reports have focused on producing uniform NTN structures to overcome these obstacles. Dharmaraj *et al.*⁶ fabricated NTN nanofibers by sol-gel processing and an electrospinning technique, following by high temperature calcination of the nickel titanate/poly(vinyl acetate) composite fibers. Ni and coworkers¹² designed a simple solution-combustion route to prepare pure NTN microtubes for the degradation of organic dyes under irradiation with 254 nm UV light. Tubes with an outer diameter of 500-600 nm, inner diameter of 400-500 nm and length ranging from 2 to 4 μm were constructed from nearly spherical nanoparticles with a mean diameter of ~50 nm. Qu *et al.*³ successfully synthesized one-dimensional (1D) porous NTN nanorods of aggregated nanoparticles in ethylene glycol at room temperature followed by pyrolysis of the metal-glycolate precursor at 600 °C in air. Nonetheless, to the best of

^a School of Chemical Engineering, University of Ulsan, Daehakro 93, Nam-gu, Ulsan 680-749, South Korea. Fax: +82 52 259 1689; Tel: +82 52 259 2253; E-mail: ewshin@mail.ulsan.ac.kr

^b Department of Chemical Engineering and Energy Systems Research, Ajou University, 206 Worldcup-ro, Yeongtong-gu, Suwon 443-749, South Korea.

† Electronic Supplementary Information (ESI) available: [Experimental detail of solvothermal synthesis, methylene blue decolorization and nitrobenzene degradation under visible light illumination. Figures S1-S5 include Tauc's plot for band gap determination, nitrobenzene photodegradation, methylene blue photodecolorization, N₂ sorption isotherm and crystal structure of NiTiO₃]. See DOI: 10.1039/x0xx00000x

our knowledge, there have been no reports in the literature concerning the shape-controlled synthesis of NiTiO₃ superstructures via a facile, energy- and cost-saving process, especially three-dimensional (3D) structures. Recently, novel rosary-like NiTiO₃ nanowire photocatalysts were prepared by an electrospinning method with the assistance of poly(vinyl pyrrolidone).¹⁸ The nanowires were single nanoparticle chains constructed of numerous randomly assembled nanograins. These studies solely focused on the synthesis of several low-dimensional morphologies of NTN and not complicated or hierarchical architectures. It has been well known that materials with 3D specific geometries are of great interest due to their unexpected, unique, and attractive properties generated from either combinative or synergistic effects, potentially stimulating the development of promising and novel applications.

Microwave radiation, electromagnetic radiation spanning the frequency range from 30 GHz to 300 MHz, has blossomed into a mature and useful technique in recent decades in academic and industrial laboratories. Relying on the frequency of 2.45 GHz (corresponding to a wavelength of 12.2 cm) available for commercial, medical, and scientific applications, microwave-assisted synthesis has received a great deal of interest for the fabrication of nanostructured materials. Numerous nanomaterials of different dimensions and morphologies have been produced under microwave exposure including zeolites, nanoparticles (CdSe, InP, CdTe, Cu_{2-x}Se, BaTiO₃), nanotubes (TiO₂, CdS), nanowires (Ag, Au, ZnS, ZnSe), nanorods (ZnS, CdSe), microspheres (BiOBr, SiO₂), flowers

(Co₃O₄), ball cactus (Cu₂ZnSnS₄), etc.²⁰⁻⁴⁴ Flash-heating *via* ionic conduction and dipole rotation from microwave energy is more advantageous to chemical synthesis compared with conventional thermal heating, *i.e.* acceleration of reaction rates, drastically shortening the total reaction time from days or hours to minutes, thus providing energy-consumption savings; generating rapid temperature increases and uniform dielectric heating patterns that may favor kinetically competent and nonequilibrium chemical processes, as well as limiting localization of heating; homogenizing nucleation, dramatically increasing the product yield/quality, and narrowing the dimension distribution of materials.^{28,33,35,38-40} Additionally, microwave energy is introduced into the chemical reactor remotely without direct contact between the energy source and the reacting chemicals, thus minimizing wall or heat diffusion effects.³²

In this regard, we report for the first time a rapid, facile one-pot synthesis of hierarchical nickel titanate nanomaterials assembled from small nanoparticles by microwave-assisting polyol processing using Ti/Ni precursor reagents and ethylene glycol. A commercially available microwave oven was used as the heating source instead of special microwave apparatus. As mentioned above, no previous work has described the unique morphological tuning of NTN nanomaterials with high purity and homogeneity based on experimental conditions; therefore, herein, we demonstrate the influence of the medium dielectric and precursor counterion on the shapes of superstructured NTN samples.

Table 1. Structural properties of hierarchical NTN nanomaterials.

Sample	Synthetic conditions	Morphology	Crystalline phase / % ^a	Unit cell parameters / Å ^b
NTN-N-H ₂ O	Ti(O-C ₄ H ₉) ₄	Irregular aggregates	A (85.5±8.8)	<i>a</i> = <i>b</i> = 3.7891, <i>c</i> = 9.5162
	Ni(NO ₃) ₂ H ₂ O		N (14.5±0.8)	<i>a</i> = <i>b</i> = 5.0284, <i>c</i> = 13.8153
NTN-N-BuOH	Ti(O-C ₄ H ₉) ₄	Irregular aggregates	A (78.1±6.5)	<i>a</i> = <i>b</i> = 3.7890, <i>c</i> = 9.5189
	Ni(NO ₃) ₂ C ₄ H ₉ OH		N (21.9±0.8)	<i>a</i> = <i>b</i> = 5.0332, <i>c</i> = 13.7959
NTN-N-AA	Ti(O-C ₄ H ₉) ₄	Skeleton-like agglomerates	N (84.9±7.4)	<i>a</i> = <i>b</i> = 5.0331, <i>c</i> = 13.7962
	Ni(NO ₃) ₂ CH ₂ =CHCO ₂ H		R (15.1±2.2)	<i>a</i> = <i>b</i> = 4.6016, <i>c</i> = 2.9731
NTN-N-DMF	Ti(O-C ₄ H ₉) ₄	Spheroidal aggregates	N (80.9±6.2)	<i>a</i> = <i>b</i> = 5.0286, <i>c</i> = 13.7691
	Ni(NO ₃) ₂ (CH ₃) ₂ NC(O)H		R (19.1±3.4)	<i>a</i> = <i>b</i> = 4.6095, <i>c</i> = 2.9746
NTN-N-EG	Ti(O-C ₄ H ₉) ₄	Cylindrical storage tank-like aggregates with elliptical end caps	N (97.2±8.7)	<i>a</i> = <i>b</i> = 5.0331, <i>c</i> = 13.8072
	Ni(NO ₃) ₂ C ₂ H ₄ (OH) ₂		R (2.8±0.9)	<i>a</i> = <i>b</i> = 4.5933, <i>c</i> = 2.9680
NTN-N-(EG:BuOH)	Ti(O-C ₄ H ₉) ₄	Hexagonal prisms with spongy inner	N (96.4±4.8)	<i>a</i> = <i>b</i> = 5.0305, <i>c</i> = 13.8156
	Ni(NO ₃) ₂ (C ₂ H ₆ O ₂ :C ₄ H ₁₀ O)		R (3.6±0.8)	<i>a</i> = <i>b</i> = 4.5966, <i>c</i> = 2.9826
NTN-A-EG	Ti(O-C ₄ H ₉) ₄	Solidified hexagonal prisms	N (97.5±8.7)	<i>a</i> = <i>b</i> = 5.0348, <i>c</i> = 13.8045
	Ni(CH ₃ COO) ₂ C ₂ H ₄ (OH) ₂		R (2.5±0.9)	<i>a</i> = <i>b</i> = 4.5936, <i>c</i> = 2.9739
NTN-C-EG	Ti(O-C ₄ H ₉) ₄	Nanorods	A (26.3±3.6)	<i>a</i> = <i>b</i> = 3.7878, <i>c</i> = 9.4940
	NiCl ₂		R (19.2±1.8)	<i>a</i> = <i>b</i> = 4.5946, <i>c</i> = 2.9557
	C ₂ H ₄ (OH) ₂		N (9.0±0.8)	<i>a</i> = <i>b</i> = 5.0319, <i>c</i> = 13.7851
			B (45.5±4.0)	<i>a</i> = 5.4494, <i>b</i> = 9.1839, <i>c</i> = 5.1451

^a Calculated from Spurr and Myers's equation,⁴⁵ A – anatase, N – nickel titanium oxide, R – rutile, B – brookite

^b Refined from XRD patterns by X Powder program (ver.2004)

Experimental

Synthesis of nickel titanate

All of the chemical reagents used in the synthesis of the materials described in this study were purchased from Sigma-Aldrich and were used as received without further purification.

In a typical synthesis procedure of NTN material in the shape of cylindrical storage tank with two elliptical end caps, a mixture containing 0.01 mol of titanium n-butoxide (TBOT, 97%), 0.01 mol of nickel (II) nitrate hexahydrate ($\text{Ni}(\text{NO}_3)_2 \cdot 6\text{H}_2\text{O}$, 99.999%, Ni-N) and 50 mL of ethylene glycol (EG, 99.8%) in a glass beaker was placed in a conventional household microwave oven (MW209QV, LG Electronics, South Korea), and the greenish solution was sonicated for 1 h. The

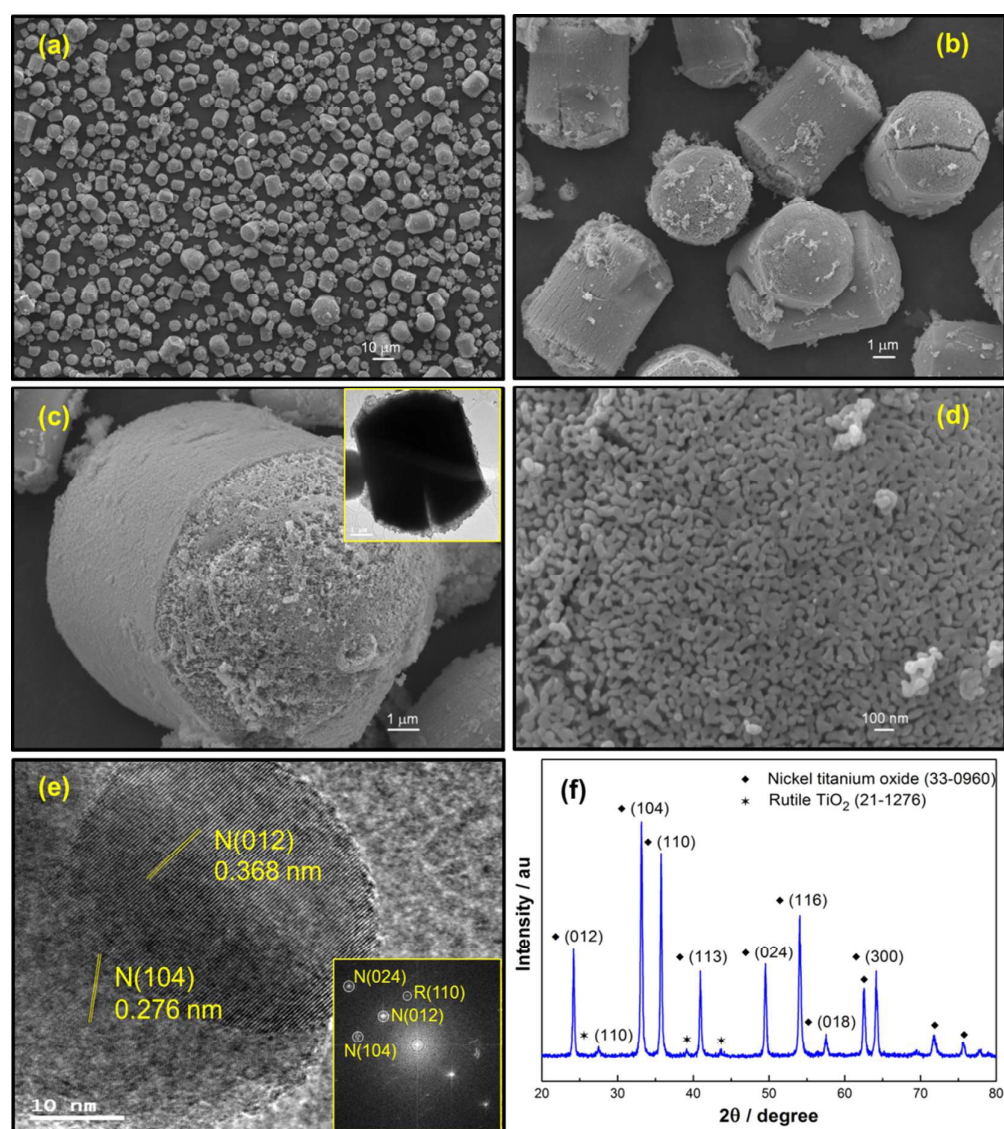


Figure 1. (a-d) FE-SEM images, (e) HR-TEM and (f) XRD pattern of NiTiO_3 aggregates in the geometry of 3D cylindrical storage tank with two elliptical end caps when prepared by microwave-assisted method, using EG and nickel nitrate as only solvent and Ni precursor, respectively. Insets of (c) and (e) are HR-TEM and FFT pattern.

maximum output power was 1050 W, and the frequency was 2.45 GHz. After cycling modes (10 first cycles, on 10 s/off 5 s; 5 second cycles, on 20 s/off 5 s) under microwave irradiation, the sample was rapidly cooled to room temperature by strong cold water fluid. The light green precipitate was washed several times with ethanol and was collected by centrifugation, followed by drying at 80 °C overnight. Finally, the solid was calcined in air at 600 °C for 5 h with a 2 °C min⁻¹ heating ramp to obtain the bright yellow nickel titanate powder (denoted as **NTN-N-EG**). A solvothermal-treated sample was also prepared for comparison (as NTN-N-EG-s). Detailed solvothermal preparation was described in ESI†.

Solvents with different dielectric constants (non-polyol), such as deionized water, n-butanol (BuOH, ≥99.4%), acrylic acid (AA, 99%), N,N-dimethylformamide (DMF, 99.8%), and a mixture of EG and BuOH (volume ratio 1:1) were investigated. Two different nickel precursor sources were also employed, including nickel (II) acetate tetrahydrate (Ni(CH₃COO)₂·4H₂O, 99.998%, Ni-A) and nickel (II) chloride (NiCl₂, 99.99%, Ni-C). All of the samples were named “**NTN-X-Y**” where X and Y indicate the Ni source and solvent, respectively, used in the synthesis procedure. A listing of all of the samples prepared using the different conditions is summarized in Table 1.

Characterization techniques

Powder X-ray diffraction (XRD) patterns were recorded on a Rigaku Ultima-IV X-ray diffractometer (Japan) with Cu K α radiation ($\lambda = 1.5418 \text{ \AA}$). Sample morphology was visualized with a field-emission scanning electron microscope (FE-SEM, JEOL JSM-600F) and a high-resolution transmission electron microscope (HR-TEM, JEOL JEM-2100F) equipped with Fast Fourier transforms (FFT) analysis. X-ray photoelectron spectra (XPS) were acquired by a K-alpha X-ray photoelectron spectrometer (Thermo Fisher, UK). UV-Vis diffuse reflectance spectra were obtained with a SPECORD® 210 Plus spectroscope (Analytikjena, Germany). The specific surface area of materials was determined with a Micromeritics ASAP

2020 instrument (USA) at -196 °C.

Results and discussion

Figure 1 shows the morphology of the NTN-N-EG sample prepared using TBOT, Ni-N, and EG with microwave irradiation. The FE-SEM micrographs in Figure 1a-c reveal uniform aggregates in the shape of a 3D cylindrical storage tank with two elliptical end caps (rounded cylinder). The cylinder length was approximately 5 ~ 10 μm , and the minor ellipse radius ranged from 800 nm to 1 μm . The magnified image clearly indicates that an individual hierarchical assembly was constructed by small ellipsoid-like nanoparticles with an average grain size of ca. 25 nm. Two sets of well-defined lattice fringes in Figure 1e with interplanar spacings of 0.368 and 0.276 nm were assigned to the (012) and (104) atomic planes, respectively, of rhombohedral NiTiO₃. Distinct spots in the FFT pattern in the inset imply the highly crystalline nature of the NTN-N-EG superstructure. The results are consistent with the crystallographic structure confirmed by XRD, shown in Figure 1f. The series of (012), (104), (110), (113), (024), and (116) diffractions was strongly detected at $2\theta = 24.1, 33.1, 35.7, 40.8, 49.4, \text{ and } 54.2^\circ$, unambiguously corresponding to rhombohedral nickel titanium oxide (JCPDS 33-0960, space group $R\bar{3}$). A small portion of rutile TiO₂ (space group $P4_2/mnm$) phase was additionally observed via the main (110) peak at 27.4° (JCPDS 21-1276). No signal for cubic bunsenite NiO or hexagonal Ni(OH)₂ was detected. The lattice constants, $a = b = 5.0331, c = 13.8072 \text{ \AA}$ for nickel titanium oxide and $a = b = 4.5933, c = 2.9680 \text{ \AA}$ for rutile, were also shown in Table 1. The mass fraction of each component was calculated from Spurr and Myers' equation on the basis of the empirical constant K and the intensity of characteristic reflections.⁴⁵ It is worth noting that the fabrication of NiTiO₃ with high uniformity and crystalline phase homogeneity has an important implication; as summarized in Table 1, the hierarchical NTN-N-EG contained 97.2 wt% of highly crystalline NiTiO₃ phase, which is much higher than other previously prepared materials.^{4,6,17} Shu et al.¹⁷ described that TiO₂ phase was observed even in the case of the Ni:Ti = 1:1 dosage in the feed of co-precipitation process because of Ni²⁺ loss during precipitation. The Ni²⁺ loss left Ti⁴⁺ in excess, resulting in the emergence of anatase TiO₂ phase. They also found that the highly dispersed NiTiO₃ crystallites efficiently prevented the anatase-to-rutile transformation even upon 800 °C calcination. Moghiminia et al.¹⁹ also obtained the mixture of NiTiO₃, anatase and rutile TiO₂ as prepared NTN with Ni:Ti molar ratio of 2:5 by low temperature modified sol-gel method. Some reports proved that the presence of impurities could be inhibited by increasing the calcination temperature from 600 to beyond 1000 °C.^{5,10,11} However, the opposite behaviour was observed in several studies where increasing post-treated temperature strongly facilitated the transformation into rutile or brookite from unreacted anatase.^{4,6} Ni et al successfully prepared highly pure microtube-shaped NiTiO₃ via a simple solution-combusting method using a spirit lamp with an absorbent cotton lampwick, following by firing with a match.¹²

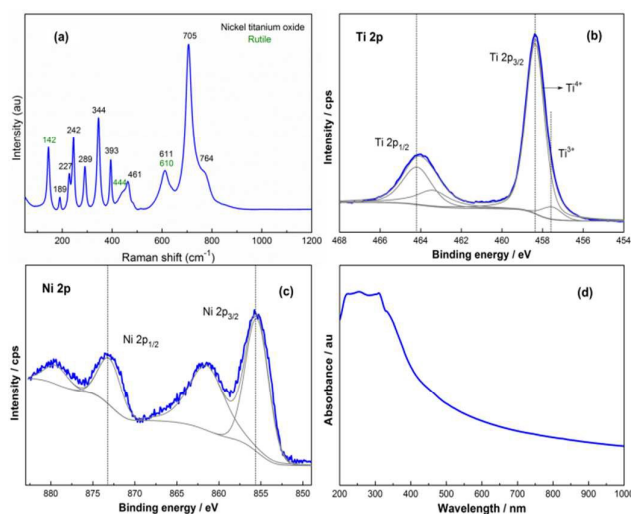


Figure 2. (a) Raman spectrum; (b, c) Ti 2p and Ni 3d core-level XPS spectra; and (d) UV-Vis-DRS spectrum.

Qu et al. achieved pure NiTiO₃ rod after pyrolysis of the metal-glycolate precursor at 600 °C without the no impurities of TiO₂ and bunsenite NiO.³ Jing et al.¹⁸ fabricated pure stoichiometric NTN nanowires (Ni:Ti = 1:1) in the rosary-like shape by the electrospinning method when annealed the wire from 700 to 1000 °C.

The highly crystalline structure of NTN-N-EG was also detected in the Raman spectrum shown in Figure 2a. Ten active modes ($5A_g+5E_g$, also named P_1 to P_{10} modes) at 189, 227, 242, 289, 344, 393, 461, 611, 705, and 764 cm^{-1} contributed to the C_{3i}^2 symmetry and $R\bar{3}$ space group of the rhombohedral ilmenite-type compound.^{11,46,47} Small shifts in the Raman band positions in this study compared with literature reports were observed, stemming from differences

structural order degree.¹¹ Two small bands were found at 143 and 444 cm^{-1} accompanied by a superimposed peak at 610 cm^{-1} , verifying the presence of rutile phase in NTN-N-EG. These results are in good agreement with the XRD analysis.

Moreover, the chemical oxidation states of NTN-N-EG determined by XPS are displayed in Figure 2b-c. The high-resolution Ti 2p XPS spectrum obviously shows binding energies of Ti 2p_{3/2} and Ti 2p_{1/2} centered at 458.4 and 464.2 eV, characteristics of octahedrally coordinated Ti⁴⁺. Small portion of lower oxidation state Ti³⁺ is also detected at 457.6 eV. Ni 2p_{3/2} and 2p_{1/2} signals for Ni²⁺ were found at 855.6 and 873.2 eV, along with two relatively broad satellites at 861.7 and 879.7 eV.^{3,48,49} Figure 2d demonstrates the optical property of NTN-N-EG by UV-Vis-DRS analysis. The absorption

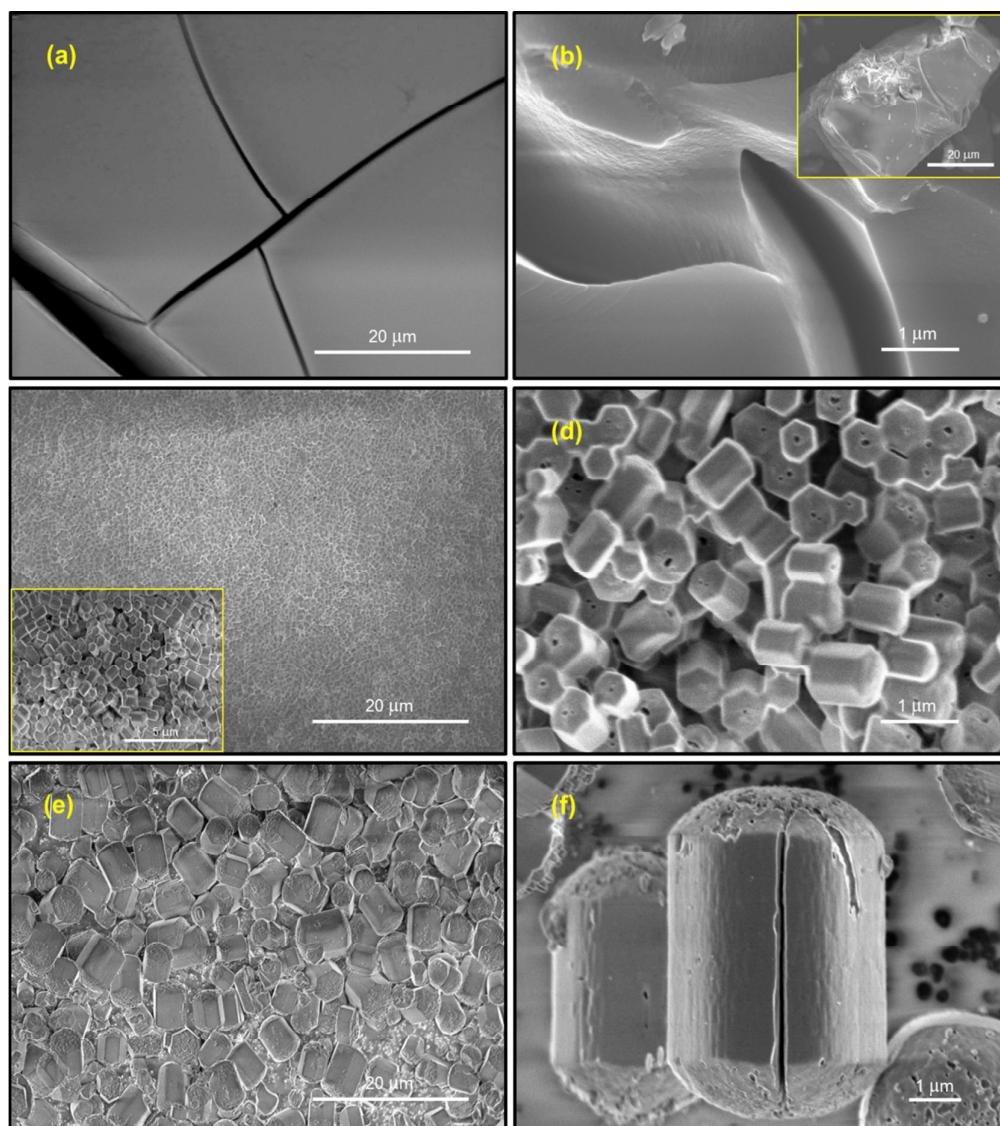


Figure 3. SEM images of the intermediate products obtained by different transition stages: (a) before microwave heating; (b) after 10 first-cycle-irradiation; (c, d) after 5 second-cycle-irradiation; and (e, f) after rapid cooling.

in the synthesis method, the average grain size, and the onset of such ternary oxide system is located at 550 nm, which

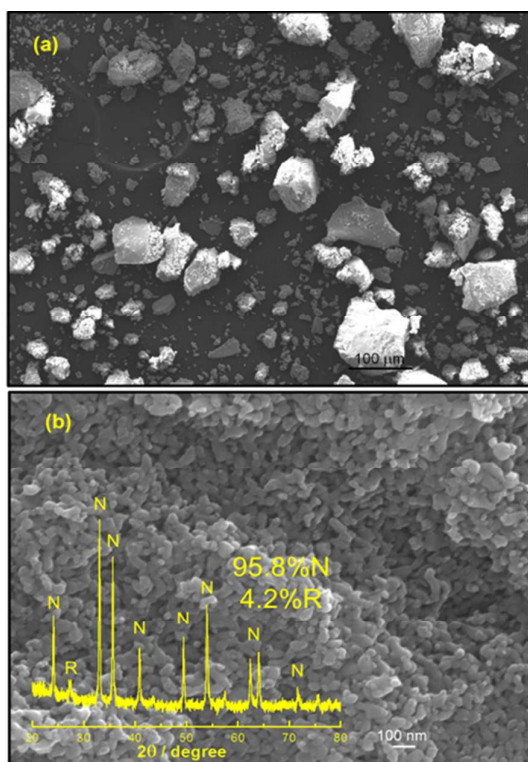


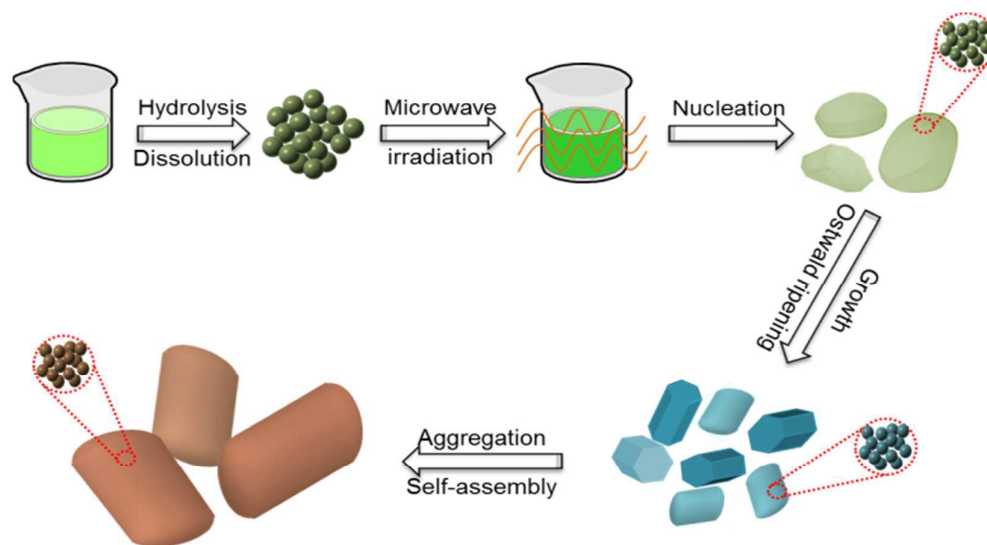
Figure 4. FE-SEM images of NiTiO_3 synthesized by solvothermal treatment at $200\text{ }^\circ\text{C}$. Inset of (b) is XRD pattern.

corresponds to band gap energy of 2.86 eV as determined by Tauc's plot in Figure S1 (see in ESI[†]). Accompanied with a long tail in the visible light region, the spectrum distinctly indicates the significantly strong photoabsorption behavior of 3D hierarchical NiTiO_3 towards both UV and visible light. It rationalizes the activity of NTN-N-EG towards the degradation of nitrobenzene and methylene blue under the irradiation of either blue LEDs ($\lambda = 450\text{--}500\text{ nm}$) or compact fluorescent

lighting ($\lambda = 400\text{--}700\text{ nm}$) (see in Figure S2 and S3 in ESI[†]).

By measuring the N_2 adsorption-desorption isotherm in Figure S4 (see in ESI[†]), the specific surface area and total pore volume of NTN-N-EG were approximately $33\text{ m}^2\text{ g}^{-1}$ and $0.193\text{ cm}^3\text{ g}^{-1}$, respectively. Such a low surface area is quite similar to several previously reported values.^{3,6,8,11,12}

The crystal growth mechanism of hierarchical NiTiO_3 under microwave irradiation was followed by the observation of intermediate products after each single steps of synthesis procedure. SEM images in Figure 3 shows the morphology of the products before microwave heating (a), after 10 first-cycle-irradiation (b), after 5 subsequent-cycle-irradiation (c, d) and after rapid cooling (e, f). It is noteworthy that uniform hexagonal prisms with average size ranging from 800 nm to $1\text{ }\mu\text{m}$ are formed after 5 second-cycling microwave radiation (on $20\text{ s/off }5\text{ s}$) whereas no special product is created during the formation of metal-glycolate complexes at room temperature and even after 10 first-cycle-exposure (on $10\text{ s/off }5\text{ s}$). Subsequent cooling step results in further growth of larger 3D as-synthesized aggregates made up of small nanoparticles. Scheme 1 illustrates the proposed model of growth evolution for hierarchical NiTiO_3 structure under microwave-assisted polyol process. Subsequent to hydrolysis and dissolution of the precursors in ethylene glycol to form titanium-nickel-glycolate complexes (Figure 3a), the microwave irradiation heated the mixture up to $\sim 198\text{ }^\circ\text{C}$ in very short periods of time ($1\text{--}3$ minutes) and the nucleation occurred (Figure 3b). The nucleation rate was remarkably accelerated, creating a large amount of crystal nuclei, and the growth process is immediately initiated. EG is a polar, protic solvent and an effective dielectric medium (dielectric constant $\epsilon = 37.7$)²⁹ that easily absorbs microwave energy due to its high dipole moment and instantaneously converts it into thermal energy, facilitating nucleus creation and further rapid nuclei growth. Herein, EG acts as the reaction and dispersion medium, a



Scheme 1. Illustration of crystal growth mechanism for hierarchical NiTiO_3 superstructures under microwave-assisted polyol process.

chelating agent, a complexing agent, and as a stabilizer due to its high viscosity.²⁴ Microwave irradiation accelerated not only nucleation but also the crystal growth. When supersaturation was relieved by nucleation, no additional nuclei were formed and these crystallites grew larger and larger. These nuclei intentionally grew in a preferred orientation (i.e. along the *c*-axis), assembling into abundant crystallites as prolonged the reaction time to 4 ~ 5 min via Ostwald ripening-assisted mechanism to minimize the total interfacial energy (Figure 3c, d). These crystallites further grew up or attached to each other though the oriented attachment associated with Ostwald ripening, transversally edge-sharing in the *ab*-plane ($a = b = 5.0331 \text{ \AA}$) and longitudinally face-sharing along the *c*-axis ($c = 13.8072 \text{ \AA}$) (as shown in Figure S5), ultimately self-assembled into hierarchical NiTiO₃ superstructures (Figure 3e, f).

The solution temperature immediately after microwave irradiation and before cooling was carefully measured to be approximately 198 °C. For comparison, a solvothermal-treated sample was prepared using the same feedstocks at 200 °C. As shown in Figure 4 irregular aggregates composed of loose granular particles were formed. Despite a composition of

95.8% NiTiO₃, material with much lower crystallinity was obtained. It is apparent that the microwave-assisted polyol process has advantages to the solvothermal method and plays a vital role in the nucleation, crystal growth, and assembly of NTN material. Contrary to the conventional heating process that transfers heat from outside the autoclave to inside the solution, microwave thermal energy is generated internally within the reactor, reversing the flow of heat and thermal gradient,¹⁹ resulting in a uniform temperature in the solution, which efficiently narrows the particle size distribution of the final products. It is known that such quick, homogeneous and *in situ* dielectric heating is created by the interaction between high frequency electromagnetic radiation and the permanent dipole moment of molecules.^{29,33,38} Thus, mechanistic variation in microwave heating versus conventional heating induces different heat interchange at microscopic level, result in the variations in size and shape of NiTiO₃.⁴⁰

The influence of rapid cooling and natural cooling on the structure of as-synthesized NTN was also considered. Obviously, more uniform geometry, narrower particle size distribution and less free particles of as-synthesized products were obtained in case of rapid cooling as seen in Figure 5. Natural cooling induces inhomogeneous temperature gradients, generating several zones with higher temperature to other zones with lower temperature. Rapid cooling helps prevent the decomposition or side reactions through quenching at the end of the synthesis and thus, enhances the yield and homogeneity of final product. Both extremely rapid heating and subsequent cooling rates could potentially lead to the fabrication of kinetic controlled phases that could not be easily obtained by other routes.²² This result is well consistent with the literature that heating and cooling could be performed simultaneously (concurrent heating and cooling), thereby reducing possibilities of thermal runaway in the case of exothermic reactions requiring heat input.^{20,26,39}

An investigation of factors influencing the NTN morphology was conducted by varying the synthetic conditions. First, instead of EG, several other solvents were employed using the same microwave-assisted protocol. As seen in Figure 6a-d, irregular aggregates consisting of large coalescent primary particles (40-50 nm) were obtained using deionized water and *n*-butanol. A skeleton-like geometry appeared with the acrylic acid medium shown in Figure 6e, f, whereas with DMF as solvent, 3D microsphere products formed. These two structures are obviously comprised of tiny nanoparticles compared to the former cases (Figure 7a, b). However, the FE-SEM image in Figure 5c clearly shows hexagonal prism microstructures resulting from using the mixture of EG and BuOH (1:1 volume ratio). The cross-sectional image clearly shows a spongy inner space comprised of hollow pores and interconnected granular channels. The hexagonal basal faces were in the range of 1-4 μm, and rectangular prism faces were built from large, nearly dendritic crystallites. The lattice fringe of the (113) plane of NiTiO₃, $d_{113} = 0.223 \text{ nm}$, is visibly depicted in Figure 7f, in agreement with the FFT pattern in the inset.

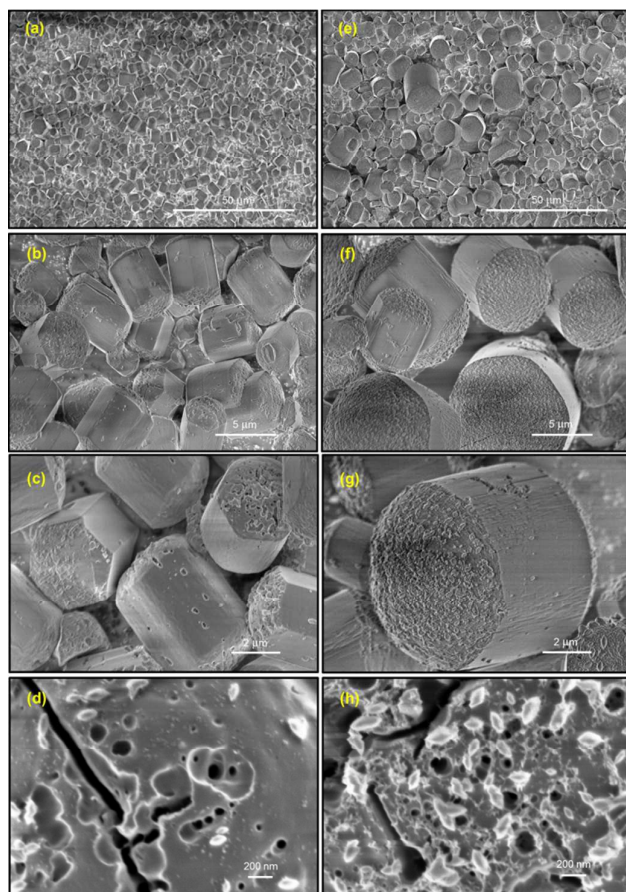


Figure 5. SEM images of as-synthesized NiTiO₃ morphology after (a-d) fast cooling and (e-h) natural cooling.

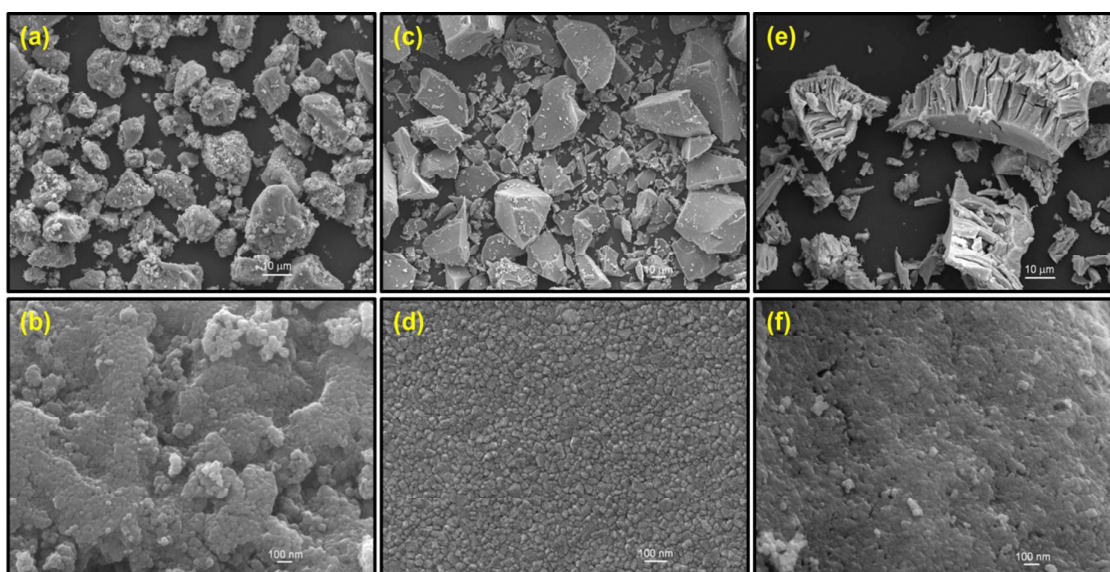


Figure 6. SEM images of as-synthesized NiTiO₃ morphology after (a-d) fast cooling and (e-h) natural cooling.

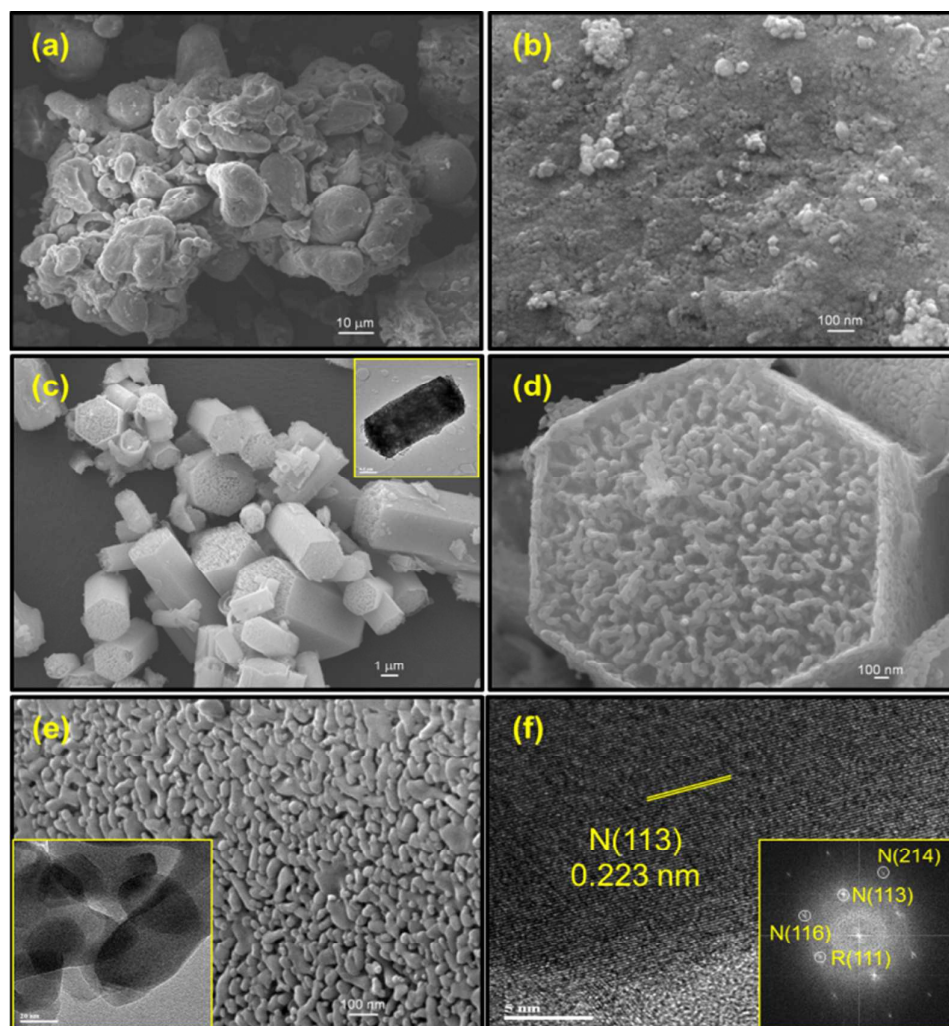


Figure 7. Morphologies of hierarchical NiTiO₃ prepared by using (a, b) DMF, (c-e) mixture of EG and n-butanol (1:1 v/v); (f) HR-TEM micrograph of NTN-N-(EG:BuOH) and inset is corresponding FFT.

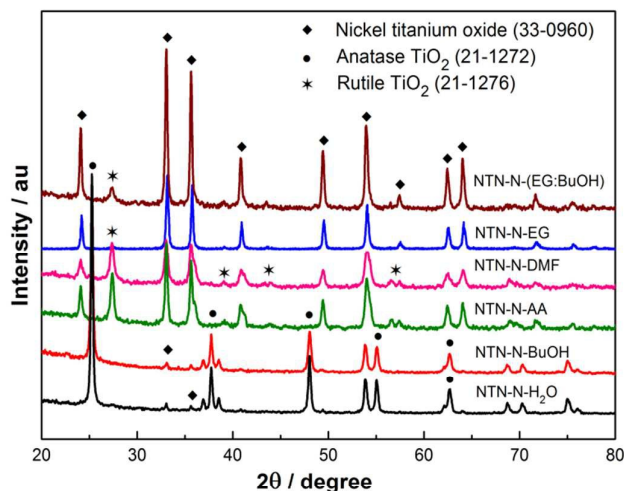


Figure 8. XRD patterns of NTN materials fabricated by different solvents upon microwave irradiation.

To investigate the crystallographic structures accompanying morphology evolution, XRD patterns of NiTiO₃ samples from different media were obtained as shown in Figure 8. It can be seen that tetragonal anatase TiO₂ with the series of (101), (004), and (200) diffractions at $2\theta = 25.4$, 37.8 , and 48.0° (JCPDS 21-1272, space group $I4_1/amd$) was mainly found in the NTN-N-H₂O and NTN-N-BuOH materials, ca. 85.5% and 78.1%, respectively, as summarized in Table 1. A trace of rhombohedral NiTiO₃ was detected in the form of (104) and (110) diffractions at $2\theta = 33.1$ and 35.7° . With AA and DMF as solvent, nickel titanate was the dominant structure (> 80%) accompanied by a small amount of either anatase or rutile phase. A much higher content of NiTiO₃, 96.4%, was achieved by replacing the single solvent with a mixture of EG and BuOH.

The lattice constants were also shown in Table 1 where the values from the samples prepared by different solvents were very close.

Thus, it is striking that the geometry and crystalline phase drastically changed with the dielectric of the medium. This result could be attributed to the difference in dipole moment, dielectric constant (or relative permittivity), viscosity, and boiling point of the solvents. The dielectric heating pattern of a sample absorbing microwave energy is remarkably influenced by the energy dissipation factor of the sample (or loss tangent), $\tan \delta$. The loss tangent is described as the ratio of the dielectric loss or loss factor of the sample (ϵ'') to the real part of the dielectric constant (ϵ'), $\tan \delta = \epsilon''/\epsilon'$,^{29,40,50} which defines the capability of a material to convert absorbed microwave energy into thermal energy at a certain frequency. The interaction between microwave energy and absorbing material in the presence of dielectric medium is partially characterized by the complex dielectric factor of the materials; the real part is the conventional dielectric constant related to its electrical polarizability, and the imaginary part is the loss factor related to dissipated energy.⁵¹ The greater the dielectric loss tangent, the lower the penetration depth of the microwave energy. Thus, a reaction medium with a higher $\tan \delta$ is required for more quickly efficient absorption and dissipation, and consequently, for rapid heating.⁵² Basically, solvents can be classified as high ($\tan \delta > 0.5$), medium ($0.1 < \tan \delta < 0.5$) and low microwave absorbing ($\tan \delta < 0.1$).⁵³ Polar solvents like water, EG, and DMF with high dielectric constants $\epsilon' = 80$, 38 and 37, respectively are microwave-active, while BuOH and AA have lower values, $\epsilon'_{\text{BuOH}} = 17.8$, $\epsilon'_{\text{AA}} = 6$.^{29,33,39,40,52,53} However, when microwaves pass into EG, due to the extremely high $\tan \delta$, *i.e.* EG = 1.35 at 2.45 GHz,^{29,40} the energy is strongly absorbed, facilitating nucleation, crystal growth, and oriented

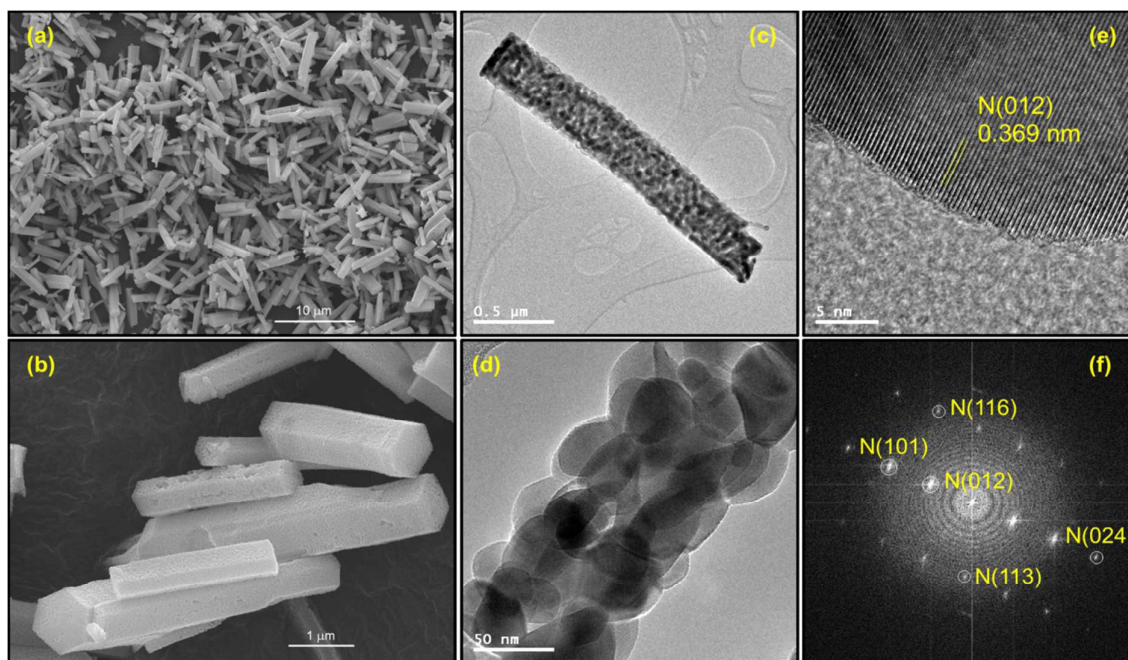


Figure 9. (a, b) FE-SEM, (c-e) HR-TEM and (f) FFT pattern of 3D hexagonal prism-like NTN-A-EG as synthesized by EG and nickel acetate.

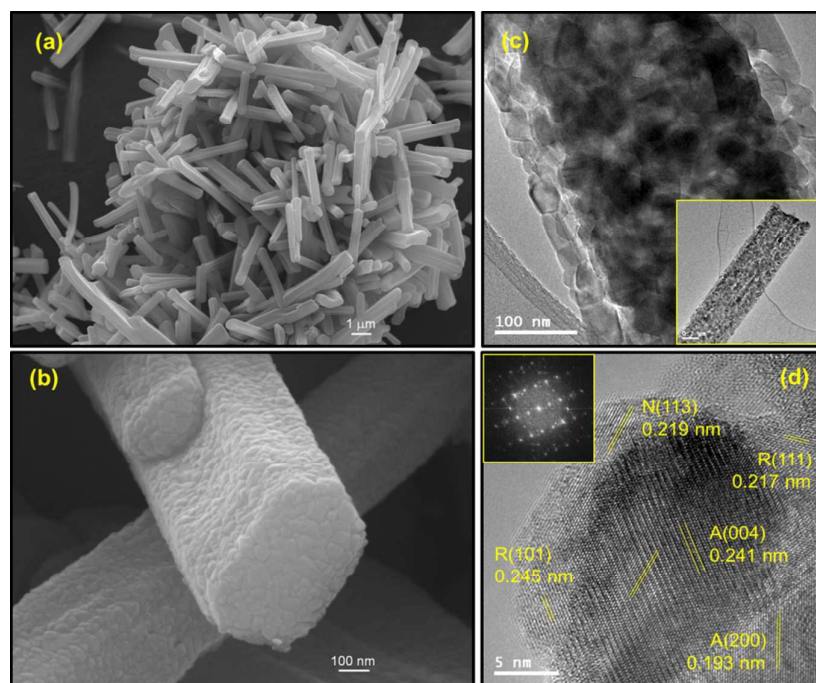


Figure 10. Nanorods assembled by small nanoparticles obtained by using EG and nickel chloride as solvent and precursor, respectively: (a, b) FE-SEM images, (c, d) HR-TEM micrographs. Inset of (d) is corresponding FFT pattern.

aggregation of rounded cylindrical NiTiO_3 clusters. In spite of the high loss tangent of BuOH, $\tan \delta = 0.571$,⁵³ the presence of either water or BuOH was predicted to rapidly accelerate the hydrolysis of alkoxide reagent and the dissolution rate at room temperature. These solvents favour the discrete nucleation of TiO_2 through the generation of abundant nuclei through the arrangement of the $[\text{TiO}_6]$ octahedral structure. Microwaves further accelerate the rate of nucleation, coalescence, crystallization, and agglomeration, giving anatase TiO_2 aggregates of macroscopic size as they fail to promote the incorporation of Ni species or the interaction between Ni and Ti components, impeding the formation of NiTiO_3 after post treatment.

In contrast, AA and DMF inefficiently absorb microwaves due to quite low $\tan \delta$ values (0.16 – 0.18), as they partially contribute to the growth of NiTiO_3 . The carboxylic acid group in AA enables the reagent to be well dispersed. AA molecules also readily self-react at their double bonds to form polyacrylic acid (homopolymer), which acts as a template for the nucleation and growth of NiTiO_3 with a skeleton-like geometry. DMF possibly plays added roles of reducing agent and chelating agent, to promote the isotropic growth of primary units to form spheroid-shaped aggregates. Further, it is obvious that the addition of BuOH into EG significantly increases the dissipation factor of the mixture as well as increases the microwave absorbability in addition to possibly affecting the boiling point and viscosity of the solution. However, an explanation for why the mixed solvent resulted in the interesting NiTiO_3 morphology remains unclear. The microwave synthesis of NTN materials using a mixed solvent requires further study in greater detail.

Apart from the medium effect, the influence of Ni counterion on the NTN morphology was studied under identical experimental conditions, *i.e.*, using microwave irradiation with EG as solvent. The microscopy observation of NTN material prepared using TBOT, EG, and nickel acetate instead of nitrate is shown in Figure 9. 3D solidified hexagonal prisms with a length of 2-3 μm were obtained that were composed of highly crystalline, closely-knit particles with diameters ranging from 30 to 40 nm (Figure 9b-d). A well-defined lattice spacing of 0.369 nm in Figure 9e is indexed to the (012) planes of rhombohedral NiTiO_3 . On the other hand, anisotropic crystal growth was also found using the halide counterion. Figure 10a shows the formation of 1D nanorods with aspect ratios (length of long sides and short sides) of 6-12. Similar to NTN-A-EG, these rods were conglomerated from coarsened particles as displayed in Figure 10b, c. However, the non-uniform contrast between the core and outer surface of the rods in the TEM image strongly relates to the density and arrangement of the structural subunits. A high-resolution image taken from the edge of the same rod and the corresponding FFT pattern in Figure 10d obviously illustrates the polycrystallinity of the rounded rectangular particles. Complicated lattice fringes were identified, including 0.241 and 0.193 nm for the anatase (004) and (200) planes; 0.245 and 0.217 nm for the rutile (101) and (111) planes, and 0.219 nm for the (113) plane of NiTiO_3 . These data are entirely compatible with the XRD patterns depicted in Figure 11 in which two major TiO_2 polymorphs were present in NTN-C-EG, 26.3% anatase and 19.2% rutile. A very low concentration of NiTiO_3 was found, along with an orthorhombic brookite TiO_2 impurity through the existence of a (121) diffraction at 30.7°

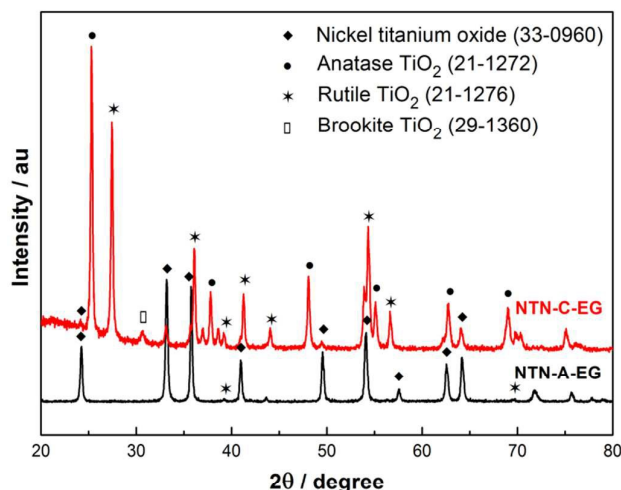


Figure 11. Influence of nickel precursor on the crystalline structure of NTN-A-EG and NTN-C-EG materials.

(*Pbca*, JCPDS 29-1360). In contrast, numerous characteristic (012), (104), (110), (113), (024), (116) and (018) reflections for ilmenite NiTiO_3 (JCPDS 33-0960) were predominantly recognized in the hexagonal prismatic sample. Rutile TiO_2 diffractions were a minority, approximately 2.5 wt%. The lattice parameters of nickel titanium oxide, rutile, anatase and brookite phases were summarized in Table 1.

It is obvious that varying the Ni counterion produced great differences in both the morphological features and the crystallographic arrangement. In all of the cases, anisotropic growth along the *c*-axis of the octahedron [MO_6] units was preferred. It is on account of the leaving group ability and coordination ability with metal ions that the counterion affects formation of the relevant nucleus. Among the three counterions, the leaving group ability increases in the order: $\text{CH}_3\text{COO}^- < \text{NO}_3^- < \text{Cl}^-$, and the corresponding basicity decreases. Thus, the halide anion strongly absorbs to the surface as well as is much more easily substituted or reacted with other chemicals in solution. However, halide detrimentally creates Cl-containing titanium hydroxo complexes through terminal coordination, preferentially speeding up nucleation and crystallization of TiO_2 from [TiO_6] octahedra, not ilmenite formation, and favors aggregation by oriented or epitaxial attachment of primary particles. Accordingly, the arrangement of octahedra [TiO_6] *via* face-shared bonding forms spiral chains and then edge-sharing (along the [100] and [010] directions), creating anatase TiO_2 ; whereas rutile phase is formed by isolated chains of octahedra along the [001] direction connected only by edges,⁵⁴ which explains the lack of NiTiO_3 phase and the generation of long 1D rod-like TiO_2 impurities that become the main products when NiCl_2 was used. While NO_3^- can coordinate with metal cations *via* a bidentate model, acetate ion, a strong base and chelating ligand, easily coordinates with metals as monodentate and chelating/bridging bidentate (chain-like glycolate complexes)⁵⁵ that proceeds crystal growth and self-assembly of the NiTiO_3 architecture in three dimensions, like rounded cylinders and

hexagonal prisms, to minimize the total interfacial energy. The behaviors of these anions are quite similar to some reports of the influence of precursor salts on the structures and morphologies of metal oxides.⁵⁵⁻⁵⁸ Taking into account that both nitrate and acetate anions induce a well-defined morphology and high purity of NiTiO_3 , it can be concluded that these counterions, but not halide, are perfectly suited to the preparation of hierarchical NiTiO_3 using the experiment conditions in this study.

Conclusions

We report a rapid and facile microwave-assisted polyol process to synthesize a novel 3D rounded cylindrical NiTiO_3 nanostructure containing small ellipsoid-like particles. The crystal growth mechanism of hierarchical NiTiO_3 superstructure upon microwave-assisted polyol synthesis was proposed through the morphology observation of intermediate products. Because of relatively narrow band gap energy, such cylindrical NiTiO_3 is a good candidate for the photocatalytic degradation of organic pollutants under visible light illumination. This microwave synthesis is superior to solvothermal treatment, which induces irregular aggregates. The influence of solvent dielectric constant and nickel counterion on the morphology and crystallographic structure of NTN were conducted. Using water and *n*-butanol led to formation of irregular anatase TiO_2 , while acrylic acid, DMF, and a mixture of EG:butanol resulted in hierarchical NiTiO_3 with skeleton, sphere and hexagonal prism with spongy inner space geometries, respectively. With acetate and halide ion instead of nitrate anion, solidified hexagonal prismatic NiTiO_3 and undesirable TiO_2 nanorods were formed. This study is expected to provide a rapid and effective method to synthesize NiTiO_3 with uniform morphology and high purity on a large scale for practical applications.

Acknowledgements

This research was supported by the Basic Science Research Program through the National Research Foundation of Korea (NRF) funded by the Ministry of Education, Science and Technology (No. 2010-0008810) and the National Research Foundation of Korea (NRF) grant funded by the Korea government (MEST) (Grant No. 2012R1A2A2A01004416).

References

1. XC. Liu, R. Hong and C. Tian, *J. Mater. Sci.: Mater. Electron.*, 2009, **20**, 323-327
2. Y. Lin, Y. Changa, G. Chen, Y. Chang and Y. Chang, *J. Alloys Compd.*, 2009, **479**, 785-790
3. Y. Qu, W. Zhou, Z. Ren, S. Du, X. Meng, G. Tian, K. Pan, G. Wang and H. Fu, *J. Mater. Chem.*, 2012, **22**, 16471-16476
4. D. J. Taylor, P. F. Fleig and R. A. Page, *Thin Solid Films*, 2002, **408**, 104-110
5. I. V. Pishch and E. V. Radion, *Glass Ceram.*, 2003, **60**, 154-157

- 6 N. Dharmaraj, H. C. Park, C. K. Kim, H. Y. Kim and D. R. Lee, *Mater. Chem. Phys.*, 2004, **87**, 5-9
- 7 V. Gupta, K. K. Bamzai, P. N. Kotru and B. M. Wanklyn, *Mater. Chem. Phys.*, 2005, **89**, 64-71
- 8 Y.-J. Lin, Y.-H. Chang, W.-D. Yang and B.-S. Tsai, *J. Non-Cryst. Solids*, 2006, **352**, 789-794
- 9 A. V. Murugan, V. Samuel, S. C. Navale and V. Ravi, *Mater. Lett.*, 2006, **60**, 1791-1792
- 10 M. S. Sadjadi, K. Zare, S. Khanahmadradeh and M. Enhessari, *Mater. Lett.*, 2008, **62**, 3679-3681
- 11 K. P. Lopes, L. S. Cavalcante, A. Z. Simões, J. A. Varela, E. Longo and E. R. Leite, *J. Alloys Compd.*, 2009, **468**, 327-332
- 12 Y. Ni, X. Wang and J. Hong, *Mater. Res. Bull.*, 2009, **44**, 1797-1801
- 13 H. Wendt and G. Imarisio, *J. Appl. Electrochem.*, 1988, **18**, 1-14
- 14 O. Yamamoto, Y. Takeda, R. Kanno and M. Noda, *Solid State Ionics*, 1987, **22**, 241-246
- 15 H. Obayashi, Y. Sakurai and T. Gejo, *J. Solid State Chem.*, 1976, **17**, 299-303
- 16 Y. Shimizu, K. Uemura, N. Miura and N. Yamazoe, *Chem. Lett.*, 1988, **17**, 1979-1982
- 17 X. Shu, J. He and D. Chen, *Ind. Eng. Chem. Res.*, 2008, **47**, 4750-4753
- 18 P. Jing, W. Lan, Q. Su, M. Yu and E. Xie, *Sci. Adv. Mater.*, 2014, **6**, 434-440
- 19 S. Moghiminia, H. Farsi and H. Raissi, *Electrochimica Acta*, 2014, **132**, 512-523
- 20 C.R. Strauss and R.W. Trainor, *Aus. J. Chem.*, 1995, **48**, 1665-1692
- 21 Y. Ma, E. Vileno, S. L. Suib and P. K. Dutta, *Chem. Mater.*, 1997, **9**, 3023-3031
- 22 J. D. Houmes and H.-C. zur Loye, *J. Solid State Chem.*, 1997, **130**, 266-271
- 23 J. Zhu, O. Palchik, S. Chen and A. Gedanken, *J. Phys. Chem. B*, 2000, **104**, 7344-7347
- 24 D. Chen, K. Tang, G. Shen, J. Sheng, Z. Fang, X. Liu, H. Zheng and Y. Qian, *Mater. Chem. Phys.*, 2003, **82**, 206-209
- 25 J. A. Gerbec, D. Magana, A. Washington and G. F. Strouse, *J. Am. Chem. Soc.*, 2005, **127**, 15791-15800
- 26 B. A. Roberts and C.R. Strauss, *Acc. Chem. Res.*, 2005, **38**, 653-661
- 27 A. B. Panda, G. Glaspell and M. S. El-Shall, *J. Am. Chem. Soc.*, 2006, **128**, 2790-2791
- 28 L. Gou, M. Chipara and J. M. Zaleski, *Chem. Mater.*, 2007, **19**, 1755-1760
- 29 J. P. Tierney and P. Lidström, *Microwave Assisted Organic Synthesis*, Blackwell Publishing Ltd, UK, 2007
- 30 Y. Ding, L. Xu, C. Chen, X. Shen and S. L. Suib, *J. Phys. Chem. C*, 2008, **112**, 8177-8183
- 31 A. L. Washington II and G. F. Strouse, *J. Am. Chem. Soc.*, 2008, **130**, 8916-8922
- 32 Y. Li and W. Yang, *J. Membr. Sci.*, 2008, **316**, 3-17
- 33 V. Polshettiwar and R. S. Varma, *Aqueous Microwave Assisted Chemistry - Synthesis and Catalysis*, RSC Green Chemistry No. 7, Royal Society of Chemistry, UK, 2010
- 34 M. N. Nadagouda, T. F. Speth and R. S. Varma, *Acc. Chem. Res.*, 2011, **44**, 469-478
- 35 L. Zhang, X.-F. Cao, X.-T. Chen and Z.-L. Xue, *J. Colloid Interface Sci.*, 2011, **354**, 630-636
- 36 D. D. Lovingood, J. R. Owens, M. Seeber, K. G. Kornev and I. Luzinov, *ACS Appl. Mater. Interfaces*, 2012, **4**, 6875-6883
- 37 W. Wang, H. Shen and X. He, *Mater. Res. Bull.*, 2013, **48**, 3140-3143
- 38 S. Horikoshi and N. Serpone, *Microwaves in Nanoparticle Synthesis - Fundamentals and Applications*, Wiley-VCH, Germany, 2013
- 39 H. J. Kitchen, S. R. Vallance, J. L. Kennedy, N. Tapia-Ruiz, L. Carassiti, A. Harrison, A. G. Whittaker, T. D. Drysdale, S. W. Kingman and D. H. Gregory, *Chem. Rev.*, 2014, **114**, 1170-1206
- 40 Y.-J. Zhu and F. Chen, *Chem. Rev.*, 2014, **114**, 6462-6555
- 41 S. Rabieh, M. Bagheri, M. Heydari and E. Badiiei, *Mater. Sci. Semicond. Process.*, 2014, **26**, 244-250
- 42 J. Zhao, Y.-J. Zhu, J. Wu and F. Chen, *J. Colloid Interface Sci.*, 2015, **440**, 39-45
- 43 X. Wang, J. Tian, C. Fei, L. Lv, Y. Wang and G. Cao, *RSC Adv.*, 2015, **5**, 8622-8629
- 44 B. You, N. Jiang, M. Sheng and Y. Sun, *Chem. Commun.*, 2015, **51**, 4252-4255
- 45 R. A. Spurr and H. Myers, *Anal. Chem.*, 1957, **29**, 760-762
- 46 M. I. Baraton, G. Busca, M. C. Prieto, G. Ricchiardi and V. S. Escribano, *J. Solid State Chem.*, 1994, **112**, 9-14
- 47 G. Busca, G. Ramis, J. M. G. Amores, V. S. Escribano and P. Piaggio, *J. Chem. Soc. Faraday Trans.*, 1994, **90**, 3181-3190
- 48 C. D. Wagner, W. M. Riggs, L. E. Davis, J. F. Moulder and G. E. Muilenberg, *Handbook of X-ray Photoelectron Spectroscopy*, Perkin-Elmer Corporation, Minnesota, USA, 1979
- 49 S.-H. Chuang, M.-L. Hsieh, S.-C. Wu, H.-C. Lin, T.-S. Chao and T.-H. Hou, *J. Am. Ceram. Soc.*, 2011, **94**, 250-254
- 50 B. Zhou, S. Hermans and G. A. Somorjai, *Nanotechnology in Catalysis (Nanostructure Science and Technology)*, Klumer Academic/Plenum Publishers, New York, 2004, vol. 1&2
- 51 W. H. Sutton, M. H. Brooks and I. I. Chabinsky, *Microwave Processing of Materials*, Materials Research Society symposium proceeding, Materials Research Society, Reno, Nevada, 1988, vol. 124
- 52 M. Larhed, C. Moberg and A. Hallberg, *Acc. Chem. Res.*, 2002, **35**, 717-727
- 53 C. O. Kappe, D. Dallinger and S. S. Murphree, *Practical Microwave Synthesis for Organic Chemists*, Wiley-VCH, Weinheim, 2009
- 54 S. B. Ogale, T. V. Venkatesan and M. G. Blamire, *Functional Metal Oxides: New Science and Novel Applications*, Wiley-VCH, Weinheim, Germany, 2013
- 55 P. K. Sharma, R. Nass and H. Schmidt, *Opt. Mater.*, 1998, **10**, 161-169
- 56 C. Force, J. P. Belzunegui, J. Sanz, A. Martínez-Arias and J. Soria, *J. Catal.*, 2001, **197**, 192-199
- 57 G. Carbajal-Franco, A. Avila-García, A. Tiburcio-Silver, D. Gouvêa and R. H. R. Castro, *J. Nanosci. Nanotechnol.*, 2010, **10**, 1338-1342
- 58 F. Behnoudnia and H. Dehghani, *Dalton Trans.*, 2014, **43**, 3471-3478.

Facile microwave-assisted synthesis and controllable architecture of three-dimensional nickel titanate

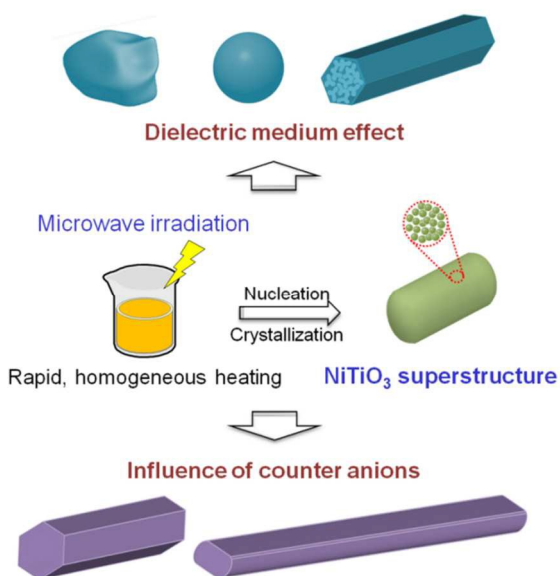
Thuy-Duong Nguyen-Phan,^a Chinh Nguyen Huy,^b Chang-Koo Kim^c and Eun Woo Shin^{*b}

^a Department of Chemistry, Brookhaven National Laboratory, POBox 5000, Upton, NY 11973-5000, USA

^b School of Chemical Engineering, University of Ulsan, Daehakro 93, Nam-gu, Ulsan 680-749, South Korea.

^c Department of Chemical Engineering and Energy Systems Research, Ajou University, 206 Worldcup-ro, Yeongtong-gu, Suwon 443-749, South Korea.

Table of contents



A rapid, facile, one-pot microwave-assisted polyol synthesis of novel hierarchical nickel titanate is first reported. The roles of medium dielectric and precursor counterion in the crystal growth and shape evolution are investigated.